RESEARCH ARTICLE
eISSN 2234-1757
Fish Aquat Sci. 2026;29(5):334-345
https://doi.org/10.47853/FAS.2026.e29
FAS Fisheries and Aquatic Sciences

Molecular characterization of glutaredoxin 5 from *Penaeus vannamei* and its potential roles in redox regulation and antibacterial defense

W. S. P. Madhuranga, Chan-Hee Kim*

Division of Fisheries Life Science, Pukyong National University, Busan 48513, Korea

Abstract

Glutaredoxin 5 (Grx5) is a member of the monothiol Grx family characterized by the conserved CGFS active-site motif and its involvement in iron–sulfur (Fe–S) cluster metabolism and cellular redox regulation. Although Grx5 proteins have been extensively studied in several model organisms, their biological roles in crustaceans remain poorly understood. In the present study, a Grx5 homolog from the white shrimp *Penaeus vannamei* (*Pv*Grx5) was identified and characterized to investigate its molecular features and potential physiological functions. The *Pv*Grx5 cDNA encodes a protein containing the conserved CGFS motif typical of monothiol Grxs. Multiple sequence alignment and phylogenetic analysis demonstrated that *Pv*Grx5 clusters with other arthropod Grx5 homologs. This result indicates strong evolutionary conservation within this lineage. Structural modeling further revealed that *Pv*Grx5 adopts a characteristic thioredoxin-like fold composed of a central β-sheet surrounded by α-helices, supporting its classification as a canonical monothiol Grx potentially involved in Fe–S cluster metabolism. Expression analysis showed that *Pv*Grx5 transcripts were detected in all examined tissues, with relatively higher expression observed in gills and hemocytes. Furthermore, *Pv*Grx5 expression was significantly upregulated following stimulation with pathogen-associated molecular patterns (PAMPs), including lipopolysaccharide (LPS), peptidoglycan (PGN), and polyinosinic:polycytidylic acid [poly(I:C)], suggesting that this gene responds to immune-related stress signals. Recombinant *Pv*Grx5 (r*Pv*Grx5) was successfully expressed in *Escherichia coli* and exhibited growth inhibitory effects against the shrimp pathogens *Vibrio harveyi* and *Lactococcus garvieae*, with a more pronounced effect observed for *L. garvieae*. Collectively, these findings provide the first molecular characterization of *Pv*Grx5 in *P. vannamei* and suggest that this monothiol Grx may participate in physiological processes linking Fe–S cluster metabolism, cellular redox regulation, and immune responses in shrimp. This study expands current knowledge of Grx-mediated redox systems in crustaceans and provides a basis for further investigations into the roles of *Pv*Grx5 in oxidative stress regulation and host defense.

Keywords: Iron–sulfur cluster metabolism, Monothiol glutaredoxin, Redox regulation, Innateimmunity, *Penaeus vannamei*

Received: Mar 10, 2026 **Revised:** Mar 12, 2026 **Accepted:** Mar 19, 2026
***Corresponding author:** Chan-Hee Kim
Division of Fisheries Life Science, Pukyong National University, Busan 48513, Korea
Tel: +82-51-629-5917, **Fax:** +82-51-629-5908, **E-mail:** chkim@pknu.ac.kr

This is an Open Access article distributed under the terms of the Creative Commons Attribution Non-Commercial License (http://creativecommons.org/licenses/by-nc/4.0/) which permits unrestricted non-commercial use, distribution, and reproduction in any medium, provided the original work is properly cited.
Copyright © 2026 The Korean Society of Fisheries and Aquatic Science

Introduction

Reactive oxygen species (ROS), including superoxide anions ($O_2^{\bullet-}$), hydrogen peroxide (H_2O_2), and hydroxyl radical (•OH), are naturally generated as inevitable byproducts of aerobic metabolism (Davies, 2000; Sies & Jones, 2020). At physiological levels, ROS act as essential signaling molecules regulating various cellular processes, including cell proliferation, differentiation, apoptosis, and innate immune responses (Sies et al., 2022). However, excessive or uncontrolled accumulation of ROS can damage nucleic acids, proteins, and lipids, resulting in cellular dysfunction, inflammation, and oxidative stress-related pathologies (Dickinson & Chang, 2011; Sies & Jones, 2020). This dual nature of ROS—serving as both indispensable regulators and potential stressors—underscores the critical importance of maintaining redox homeostasis in aerobic organisms.

The impact of oxidative stress varies markedly depending on an organism's habitat and environmental conditions. Aquatic animals are generally more susceptible to oxidative stress than terrestrial organisms, primarily due to the physicochemical instability of aquatic environments, including temperature fluctuations, hypoxia, and deteriorating water quality conditions (Di Giulio et al., 1989). The whiteleg shrimp (*Penaeus vannamei*) is one of the most commercially significant and widely farmed crustaceans worldwide, valued for its rapid growth and high environmental adaptability (Liao & Chien, 2011). However, intensive aquaculture practices impose recurrent environmental and pathogenic challenges, rendering the species vulnerable to ROS overproduction and impaired physiological homeostasis (Duan et al., 2017, 2025; Fan et al., 2022a; Parrilla-Taylor & Zenteno-Savín, 2011; Xu et al., 2018). Given the economic importance and biological sensitivity of *P. vannamei*, elucidating its antioxidant defense mechanisms is essential for enhancing disease resilience and promoting sustainable aquaculture.

To counteract oxidative damage, organisms have evolved sophisticated antioxidant systems composed of enzymatic and non-enzymatic components (Davies, 2000). Major enzymatic antioxidants include superoxide dismutase (SOD), catalase (CAT), glutathione peroxidases (GPx), and glutaredoxins (Grxs). While SOD, CAT, and GPx directly detoxify ROS, Grxs regulate cellular redox balance by catalyzing thiol-disulfide exchange reactions and the deglutathionylation of protein-glutathione (GSH) mixed disulfides. Animal Grxs are typically classified into two types based on their active site motifs: dithiol Grxs (CXXC), such as Grx1 and Grx2, which primarily reduce protein disulfides, and monothiol Grxs (CXXS or similar), such as Grx3 and Grx5, which are associated with iron-sulfur (Fe–S) cluster biogenesis and iron metabolism (Begas et al., 2017; Lillig et al., 2008; Trnka et al., 2020).

Among these, monothiol Grx5 plays a pivotal role in maintaining mitochondrial metabolic integrity. Grx5 is an essential component of the mitochondrial iron-sulfur cluster (ISC) assembly machinery, facilitating the maturation of Fe–S cluster-dependent enzymes that are vital for respiratory chain function and cellular iron sensing (Bellı et al., 2002; Johansson et al., 2011). In crustaceans, studies on Grxs have expanded to include species like the mud crab (*Scylla paramamosain*) and black tiger shrimp (*Penaeus monodon*), highlighting their roles in stress adaptation and immune signaling (Cheng et al., 2022; Fan et al., 2022b). In *P. vannamei*, although Grx2 and Grx3 homologs have been identified, the molecular characterization and immune-related functions of Grx5 are still limited in our understanding of mitochondrial homeostasis in this species.

In the present study, we aimed to clone and characterize the full-length cDNA of *P. vannamei* Grx5 (designated as *Pv*Grx5) and analyzed its structural features. The tissue-specific expression pattern of *Pv*Grx5 and its transcriptional responses to immune stimulation with pathogen-associated molecular patterns (PAMPs), including lipopolysaccharide (LPS), peptidoglycan (PGN), and polyinosinic–polycytidylic acid [poly(I:C)], were investigated. Furthermore, the antibacterial activity of r*Pv*Grx5 was evaluated against the shrimp pathogens *Vibrio harveyi* and *Lactococcus garvieae*. These results provide new insights into the potential role of mitochondrial Grx in oxidative stress regulation and innate immune defense in shrimp.

Materials and Methods

Experimental animals and tissue sampling

Healthy juvenile whiteleg shrimp (*P. vannamei*) were obtained from a commercial shrimp farm located in Muan-gun, Jeollanam-do, Korea, and acclimated in a recirculating aquaculture system (RAS) at the experimental facility of Pukyong National University. The rearing tank (width × depth × height: 1.0 × 3.0 × 0.5 m) was supplied with UV-sterilized, filtered, and aerated seawater. Water temperature and pH were maintained at 24 ± 1℃ and 7.3–7.8, respectively, with dissolved oxygen levels maintained at 9.7 ± 0.2 mg/L. Approximately 50% of the rearing water was replaced weekly using seawater treated under identical conditions. Shrimp were fed four times daily with a commercial diet (Jeil Feed, Daejeon, Korea).

Shrimp used in all experiments weighed 3.0 ± 0.5 g and measured 2.5 ± 0.3 cm in length. Hemolymph was collected using a sterile syringe pre-coated with Alsever's solution (Sigma-Aldrich, St. Louis, MO, USA) at a 1:1 ratio and centrifuged at 8,000×g for 15 min at 4℃ to isolate hemocytes. In addition, six tissues (gill, heart, hepatopancreas, lymphoid organ, muscle, and stomach) were dissected and preserved in ribonucleic acid (RNA)later solution (Invitrogen) at −80℃ until RNA extraction. As *P. vannamei* is an invertebrate species, formal ethical approval was not required; however, all procedures were conducted in accordance with the institutional guidelines of Pukyong National University.

RNA extraction, cDNA synthesis, and cloning of *Penaeus vannamei* glutaredoxin 5 (*Pv*Grx5)

Total RNA was extracted from pooled tissues (~30 mg per tissue) obtained from five healthy shrimp using the EZ™ Total RNA Miniprep Kit (Enzynomics, Daejeon, Korea) according to the manufacturer's instructions. RNA quality and concentration were assessed using a Nanophotometer NP80 (Implen, München, Germany). Only RNA samples with A260/280 and A260/230 ratios greater than 1.9 were used for subsequent analyses. For rapid amplification of cDNA ends (RACE), equal quantities of RNA from different tissues were pooled, and 1 μg of total RNA was used to synthesize RACE-ready cDNA using the SMARTer RACE 5'/3' Kit (Clontech Laboratories, San Jose, CA, USA) and the 3' RACE System (Invitrogen, Carlsbad, CA, USA). For gene expression analysis, first-strand cDNA was synthesized from 1 μg total RNA using the TOPscript™ cDNA Synthesis Kit (Enzynomics). Gene-specific primers were designed based on an in-house *P. vannamei* transcriptomic database. Primer sequences and their respective applications for RACE, cloning, and reverse transcription-quantitative polymerase chain reaction (RT-qPCR) analyses are summarized in Table 1. Touchdown PCR and nested PCR were performed to obtain the full-length cDNA sequence of *Pv*Grx5. The open reading frame (ORF) was amplified using gene-specific primers, and PCR products were cloned into the pTOP TA V2 vector (Enzynomics). Positive clones were sequenced bidirectionally (Cosmogenetech, Seoul, Korea), and the resulting sequences were assembled using BioEdit v7.2.5 to determine the full-length *Pv*Grx5 cDNA sequence.

Table 1. Primers used for cDNA cloning and expression analysis of *Pv*Grx5

Primer name	Sequence (5'–3')	Purpose
3' RACE-1	AGTGCACAAGTCGGAAGTAAA	RACE PCR
3' RACE-2	GACAGTGTTCGACAAGGGATTA	
5' RACE-1	CTGAGGTGATGCCAACTTTCT	
5' RACE-2	CTTGTGGAATTGTTGGCCAGTCTG	
*Pv*Grx5 qPCR-F	GTTGGCATCACCTCAGCCTTATT	RT-qPCR
*Pv*Grx5 qPCR-R	AAGCCTTGTACCTGAACCTATGG	
*Pv*EF1α qPCR-F	TCGCCGAACTGCTGACCAAGA	
*Pv*EF1α qPCR-R	CCGGCTTCCAGTTCCTTACC	
ORF (TA-clone)-F	CCAGGCGTAAACACTTTCCT	ORF cloning
ORF (TA-clone)-R	CAAGCCTTGTACCTGAACCTATG	
*Pv*Grx5-Exp-F[1)]	cacacaAAGCTTTGCAGTGCACAAGTCGGA	Recombinant protein expression
*Pv*Grx5-Exp-R[1)]	ctctctGAATTCTCATTTCTTTTCTCCTTT	

[1)] Lowercase letters indicate the protective bases, and the sequences AAGCTT and GAATTC correspond to the restriction sites for *HindIII* and *EcoRI*, respectively.
*Pv*Grx5, *Penaeus vannamei* glutaredoxin 5; RACE, rapid amplification of cDNA ends; PCR, polymerase chain reaction; RT-qPCR, reverse Transcription-quantitative polymerase chain reaction; ORF, open reading frame; TA, Taq DNA polymerase.

In silico sequence and phylogenetic analyses

The putative ORF and deduced amino acid sequence of *Pv*Grx5 were predicted using the NCBI ORF finder tool (https://www.ncbi.nlm.nih.gov/orffinder). Theoretical isoelectric point (pI) and molecular weight (MW) were computed using the ExPASy pI/Mw tool (https://web.expasy.org/compute_pi/), while conserved domain architectures and motif sequences were analyzed using the Conserved Domain Database (CDD; https://www.ncbi.nlm.nih.gov/Structure/cdd/wrpsb.cgi) (Marchler-Bauer et al., 2015). The potential subcellular localization and the presence of a mitochondrial transfer peptide (MTP) were evaluated using subCELlular LOcalization predictor (CELLO) v.2.5 (http://cello.life.nctu.edu.tw/) and TargetP-2.0 (https://services.healthtech.dtu.dk/services/TargetP-2.0/) (Almagro Armenteros et al., 2019; Yu et al., 2014). To investigate the structural features and GSH binding mechanism of PvGrx5, the three-dimensional (3D) structure of the mature protein (excluding the N-terminal mitochondrial targeting peptide; 125 amino acids) was predicted using the Boltz-1 (AlphaFold3) architecture implemented on the Neurosnap platform (https://neurosnap.ai/). GSH was included as a ligand during modeling to predict potential catalytic and binding orientations. Structural confidence was evaluated using the predicted local distance difference test (pLDDT) and predicted aligned error (PAE) scores. The final structural model and the CGFS catalytic motif were visualized using the PyMOL Molecular Graphics System (Version 3.0, Schrödinger, New York, NY, USA).

https://doi.org/10.47853/FAS.2026.e29

Representative Grx5 orthologs were selected primarily from decapod crustaceans, together with several non-crustacean arthropods, to clarify the phylogenetic position of *Pv*Grx5 within Arthropoda. Multiple sequence alignment (MSA) of Grx5 orthologs was performed using Clustal Omega (https://www.ebi.ac.uk/jdispatcher/msa) to examine conserved sequence features. For phylogenetic reconstruction, the conserved mature protein regions were used to improve alignment quality and minimize noise associated with variable N-terminal targeting sequences. The phylogenetic tree was reconstructed using the Maximum Likelihood (ML) method implemented in MEGA 11 (Tamura et al., 2021). The LG+G substitution model was selected as the best-fit evolutionary model according to the Bayesian Information Criterion (BIC). The reliability of the tree nodes was assessed with 1,000 bootstrap replicates.

Tissue distribution and immune-responsive expression analysis

To examine the transcriptional profiles of *Pv*Grx5, RT-qPCR was performed using the LightCycler 480 system (Roche, Rotkreuz, Switzerland) with TOPreal qPCR 2X PreMix (Enzynomics). For the immune challenge, shrimp (n = 30 per group) were intramuscularly injected with 10 μL of LPS, PGN, poly(I:C), or phosphate buffered saline (PBS) (control). Based on the tissue distribution results, gill tissue was utilized for temporal expression analysis at 0, 6, 12, 24, and 48 hours post-injection (hpi). *P. vannamei* elongation factor 1α (*Pv*EF1α) served as the internal reference (Mai et al., 2021). Relative quantification was determined using the $2^{-\Delta CT}$ (tissue distribution) and $2^{-\Delta\Delta CT}$ (immune challenge) methods (Schmittgen & Livak, 2008).

Recombinant expression and growth inhibitory activity of recombinant *Penaeus vannamei* glutaredoxin 5 (r*Pv*Grx5)

The coding sequence of mature *Pv*Grx5 was amplified using primers containing *HindIII* and *EcoRI* restriction sites and cloned into the pET-28a(+) expression vector. The recombinant plasmid was transformed into *E. coli* Rosetta (DE3) cells for protein production. Cultures were grown in LB medium containing 30 μg/mL kanamycin at 37℃ until the OD_{600} reached 0.4, after which the temperature was reduced to 18℃. Upon reaching an OD_{600} of 0.6, protein expression was induced with 0.2 mM Isopropyl β-D-1-thiogalactopyranoside (IPTG) for 15 hours. Cells were harvested by centrifugation and lysed by sonication. The His-tagged r*Pv*Grx5 was purified from the clarified lysate using HisPur nickel-nitrilotriacetic acid (Ni-NTA) resin (Thermo Scientific, Waltham, MA, USA). Protein purity was confirmed by 12% sodium dodecyl sulfate-polyacrylamide gel electrophoresis (SDS-PAGE), and protein concentration was estimated using bovine serum albumin (BSA) as a standard.

Subsequently, the growth inhibitory activity of r*Pv*Grx5 was assessed against two representative bacterial pathogens following a previously described method with minor modifications (Sun et al., 2019). Briefly, single colonies of *V. harveyi* strain FP8370 and *L. garvieae* American Type Culture Collection (ATCC) 49156 were cultured overnight at 30℃ in LB broth with shaking at 150 rpm. Culture was harvested by centrifugation at 6,000×g for 10 min at 4℃, washed once with PBS (pH 7.4), and adjusted to an OD_{600} of 1.0. The bacterial suspensions were then diluted 1:100 in fresh LB broth, and purified r*Pv*Grx5 protein was added at final concentration of 0, 50, 100, and 200 μg/mL. Bacterial growth was monitored at 1-h intervals for 10 h by measuring OD_{600}.

Statistical analysis

All data are presented as means ± SD from three independent biological replicates (n = 3). Statistical analysis was performed using one-way analysis of variance (ANOVA), followed by Tukey's honestly significant difference (HSD) post hoc test using IBM SPSS Statistics version 25. A *p*-value of less than 0.05 was considered to indicate statistical significance.

Results

Molecular and structural characterization of *Penaeus vannamei* glutaredoxin 5 (*Pv*Grx5)

The full-length cDNA of *Pv*Grx5 was 744 bp, consisting of a 76 bp 5'-untranslated region (5'-untranslated region [UTR]), a 441 bp ORF, and a 227 bp 3'-UTR (Fig. 1). The *Pv*Grx5 nucleotide sequence has been deposited in GenBank under accession number PP716118. The ORF encodes a protein of 146 amino acids with a predicted molecular weight of 16,338.75 Da and an isoelectric point (pI) of 5.90. A canonical polyadenylation signal (AATAAA) was identified 26 bp upstream of the poly(A) tail within the 3'-UTR.

Analysis of the deduced amino acid sequence using the NCBI CDD revealed a highly conserved GRX_ protein kinase C-interacting cousin of thioredoxin (PICOT)_like domain (accession: cd03028; E-value: 6.19×10^{-60}) spanning residues 33–120 (Fig. 1). This domain places *Pv*Grx5 within the thioredoxin

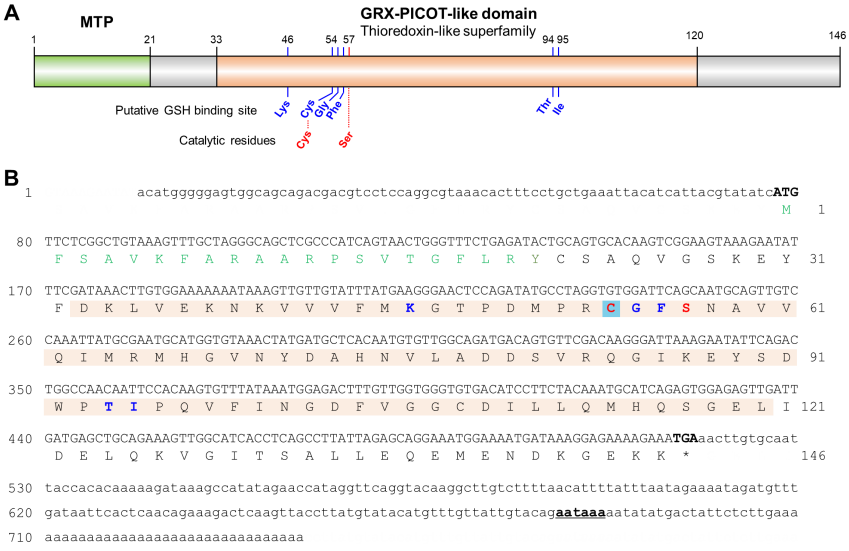

Fig. 1. Structural organization and nucleotide sequence of white shrimp *Pv*Grx5. (A) Schematic representation of the domain architecture of *Pv*Grx5. (B) Full-length cDNA and deduced amino acid sequence of *Pv*Grx5. Predicted structural features, including the CGFS active-site motif, the Grx domain, and conserved residues involved in GSH-dependent redox activity, are indicated. GRX-PICOT, glutaredoxin-protein kinase C-interacting cousin of thioredoxin; GSH, glutathione; *Pv*Grx5, *Penaeus vannamei* glutaredoxin 5; CGFS, cysteine-glycine-phenylalanine-serine; Grx, glutaredoxin.

(Trx)-like superfamily, consistent with the characteristics of monothiol Grx involved in mitochondrial Fe–S cluster transfer. The catalytic center contains a conserved CGFS motif (Cys^{54}–Ser^{57}), a signature feature of Grx5 orthologs. In addition, several putative GSH-binding residues were identified, including Lys^{46}, Cys^{54}, Gly^{55}, Phe^{56}, Thr^{94}, and Ile^{95}.

Subcellular localization prediction indicated that *Pv*Grx5 possesses an N-terminal mitochondrial targeting peptide (MTP). TargetP-2.0 predicted an MTP spanning residues 1–21 with a likelihood score of 0.9973 and a putative cleavage site between Tyr^{21} and Cys^{22}. CELLO analysis predicted cytoplasm as the primary localization category with mitochondria as the secondary localization, suggesting mitochondrial targeting of *Pv*Grx5.

The 3D structure of mature *Pv*Grx5 was modeled using Boltz-1 (AlphaFold3) and validated by structural superimposition with the human mitochondrial Grx5 crystal structure (Protein Data Bank identifier [PDB ID]: 2WUL) (Johansson et al., 2011). The predicted *Pv*Grx5 model showed high structural similarity to the human ortholog, with a root-mean-square deviation (RMSD) of 0.507 Å across 661 atoms (Fig. 2A). The overall structure exhibited the characteristic Trx-like fold, consisting of a central four-stranded β-sheet surrounded by three α-helices (Fig. 2B). Detailed structural analysis revealed the spatial arrangement of the conserved CGFS catalytic motif (residues 33–36 of mature protein, corresponding to 54–57 in full-length sequence) within the active site (Fig. 2C). In this motif, Cys^{33} (Cys^{54}) and Ser^{36} (Ser^{57}) constitute the catalytic residues. The predicted GSH-binding residues—including Lys^{25} (Lys^{46}), Cys^{33} (Cys^{54}), Gly^{34} (Gly^{55}), Phe^{35} (Phe^{56}), Thr^{73} (Thr^{94}), and Ile^{74} (Ile^{95})—were positioned in close proximity to the CGFS motif, forming a putative GSH-binding pocket.

Sequence alignment and phylogenetic analysis of *Penaeus vannamei* glutaredoxin 5 (*Pv*Grx5)

MSA was performed to examine the sequence conservation of *Pv*Grx5 with representative Grx5 orthologs from crustaceans, insects, and vertebrates (Fig. 3A). The alignment showed that the GRX-PICOT-like domain was highly conserved among all examined species. In particular, the characteristic cysteine-glycine-phenylalanine-serine (CGFS) catalytic motif of monothiol Grxs was completely conserved across the aligned sequences, indicating that the catalytic center of *Pv*Grx5 is evolutionarily conserved. Several residues associated with GSH binding, including Lys^{25}, Cys^{33}, Gly^{34}, Phe^{35}, Thr^{73}, and Ile^{74}, were also conserved among the examined Grx5 orthologs. In

https://doi.org/10.47853/FAS.2026.e29

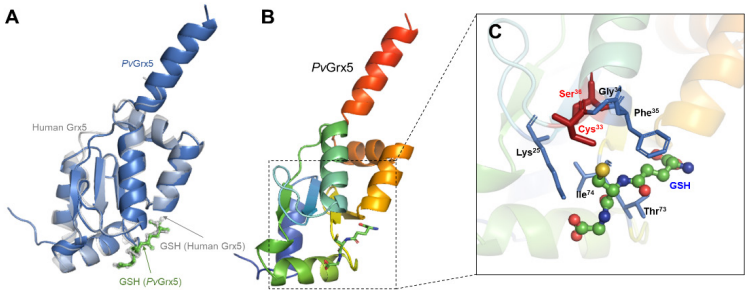

Fig. 2. Structural model of *Pv*Grx5 predicted by *in silico* modeling. (A) Superimposition of the *Pv*Grx5 with human Grx5 (PDB ID: 2WUL), illustrating the structural conservation of the catalytic region. (B) Predicted three-dimensional structure of *Pv*Grx5 showing the characteristic thioredoxin-like fold composed of a central β-sheet surrounded by α-helices. (C) Enlarged view of the CGFS active-site motif located within the catalytic pocket, which is involved in Fe–S cluster coordination in monothiol Grxs. *Pv*Grx5, *Penaeus vannamei* glutaredoxin 5; PDB ID, Protein Data Bank identifier; CGFS, cysteine-glycine-phenylalanine-serine; Fe–S, iron–sulfur.

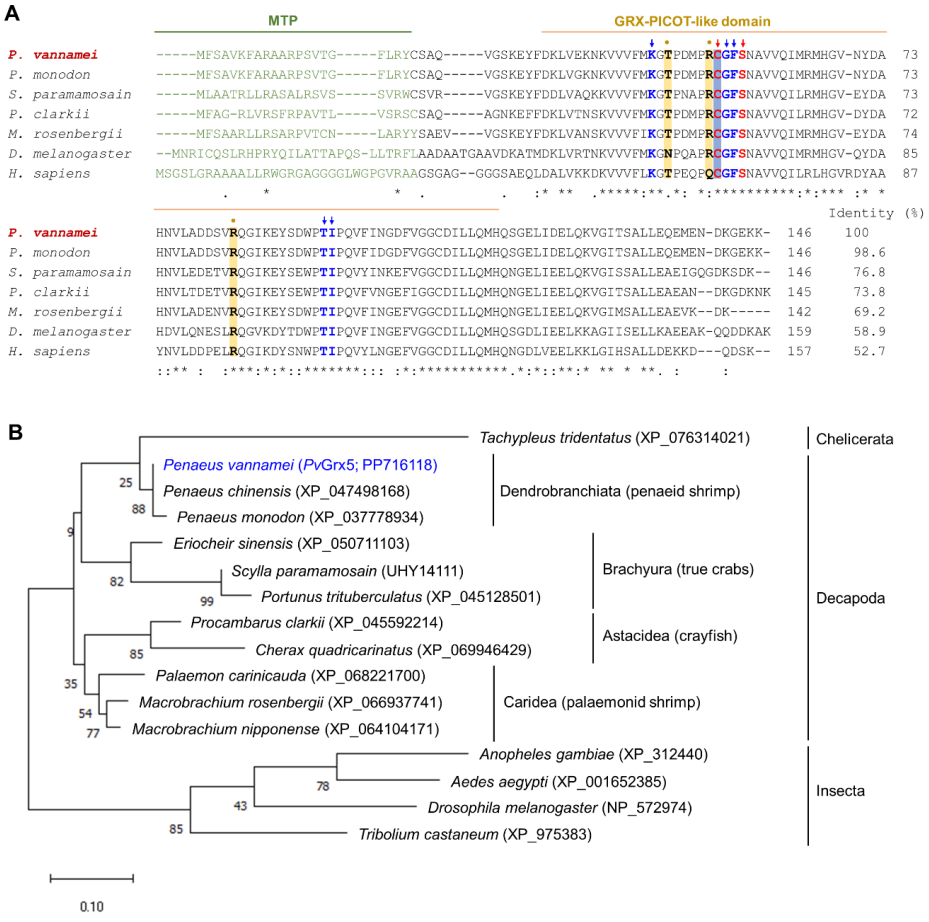

Fig. 3. Sequence conservation and phylogenetic relationship of *Pv*Grx5. (A) MSA of *Pv*Grx5 with representative Grx5 orthologs from crustaceans, insects, and vertebrates. (B) Phylogenetic tree reconstructed using the ML method based on conserved mature Grx5 protein sequences. The numbers at the nodes represent bootstrap values (1,000 replicates). MTP, mitochondrial transfer peptide; GRX-PICOT, glutaredoxin-protein kinase C-interacting cousin of thioredoxin; *Pv*Grx5, *Penaeus vannamei* glutaredoxin 5; MSA, multiple sequence alignment; ML, maximum likelihood.

addition, residues corresponding to Thr[48], Arg[53], and Arg[83], which have been reported to be involved in Fe–S cluster coordination in other Grx5 proteins, were also present in *Pv*Grx5 (Banci et al., 2014; Johansson et al., 2011; Yeung et al., 2011). These results indicate that *Pv*Grx5 shares the conserved sequence features characteristic of mitochondrial Grx5 proteins. Sequence identity analysis showed that *Pv*Grx5 exhibited the highest similarity to the penaeid shrimp *P. monodon* (98.6%), whereas lower similarity was observed with more distantly related species such as *Homo sapiens* (52.7%).

To further investigate the evolutionary relationship of *Pv*Grx5, a phylogenetic tree was reconstructed using the ML method based on conserved mature protein sequences (Fig. 3B). The phylogenetic tree showed that *Pv*Grx5 clustered with other decapod crustacean Grx5 orthologs. Within this group, *Pv*Grx5 formed a clade with *P. monodon*, consistent with the high sequence similarity observed in the alignment. Decapod Grx5 proteins were clearly separated from insect and vertebrate orthologs, reflecting the overall evolutionary relationships among these taxa.

Tissue distribution and transcriptional response of *Penaeus vannamei* glutaredoxin 5 (*Pv*Grx5) to immune challenges

To examine the tissue distribution of *Pv*Grx5, its basal expression levels were analyzed in different tissues of *P. vannamei* using RT-qPCR. *Pv*Grx5 transcripts were detected in all examined tissues, although expression levels differed significantly among tissues (Fig. 4A). The highest basal expression was observed in the gills, followed by the hemocytes and hepatopancreas. Moderate expression levels were detected in the lymphoid organ and stomach, whereas relatively lower expression was observed in the heart and muscle.

The transcriptional response of *Pv*Grx5 in the gills was further examined following stimulation with PAMPs, including LPS, PGN, and poly(I:C) (Fig. 4B). *Pv*Grx5 expression was significantly upregulated in response to bacterial mimics (LPS and PGN). At 6 hpi, *Pv*Grx5 transcript levels increased to 4.94-fold and 5.91-fold in the LPS- and PGN-treated groups ($p < 0.05$), respectively. *Pv*Grx5 expression reached a peak at 12 hpi in all challenged groups, with the highest expression observed in the PGN-treated group (12.68-fold), followed by LPS (7.90-fold) and poly(I:C) (3.75-fold). Following the peak, *Pv*Grx5 expression gradually declined at later time points. At 24 hpi, transcript levels decreased to 2.76-fold in the LPS group and returned close to basal levels in the PGN group (0.91-fold), whereas poly(I:C) stimulation resulted in reduced expression (0.47-fold). By 48 hpi, *Pv*Grx5 expression was markedly downregulated in all challenged groups, decreasing to 0.42-, 0.59-, and 0.10-fold in the LPS-, PGN-, and poly(I:C)-treated groups, respectively. These results indicate that *Pv*Grx5 is rapidly induced during early immune responses particularly in response to bacterial PAMPs.

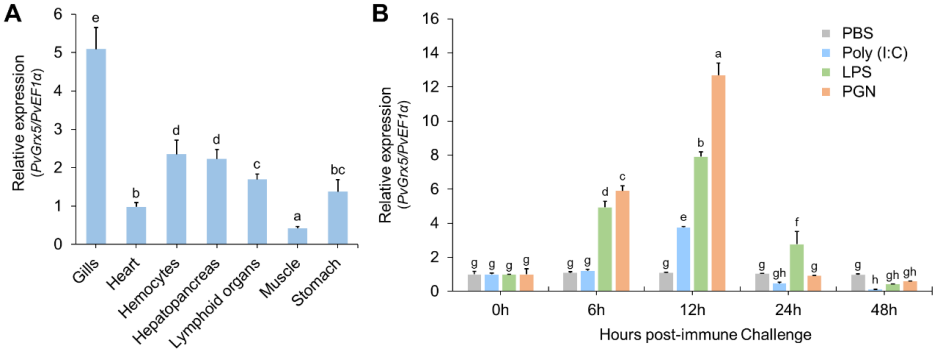

Fig. 4. Tissue-specific distribution and immune-responsive expression of *Pv*Grx5. (A) Basal mRNA expression levels of *Pv*Grx5 in various tissues of healthy *Penaeus vannamei* analyzed by RT-qPCR. (B) Temporal expression profiles of *Pv*Grx5 in the gills following PAMPs stimulation including LPS, PGN, and poly(I:C). PBS injection served as the control group. Data are expressed as mean ± SD (n = 3). Different letters indicate significant differences among all experimental groups ($p < 0.05$) based on one-way ANOVA followed by Tukey's HSD post-hoc test. *Pv*Grx5, *Penaeus vannamei* glutaredoxin 5; *Pv*EF1α, *Penaeus vannamei* elongation factor 1α; PBS, phosphate buffered saline; poly(I:C), polyinosinic–polycytidylic acid; LPS, lipopolysaccharide; PGN, peptidoglycan; RT-qPCR, reverse transcription-quantitative polymerase chain reaction; PAMPs, pathogen-associated molecular patterns; ANOVA, analysis of variance; HSD, honestly significant difference.

https://doi.org/10.47853/FAS.2026.e29

Recombinant expression and bacterial growth inhibitory activity of recombinant *Penaeus vannamei* glutaredoxin 5 (r*Pv*Grx5)

r*Pv*Grx5 was expressed in *E. coli* as an N-terminal His-tagged protein. SDS-PAGE analysis revealed a distinct band at approximately 17 kDa in the lysate and supernatant fractions, and the purified protein sample showed a band at the same position, consistent with the expected size of r*Pv*Grx5 (Fig. 5A).

The growth inhibitory activity of r*Pv*Grx5 was evaluated against the shrimp pathogens *V. harveyi* and *L. garvieae*. As shown in Fig. 5B and 5C, r*Pv*Grx5 suppressed the growth of both bacterial species in a concentration-dependent manner compared with the PBS control. In the *V. harveyi* assay, the untreated control exhibited a typical bacterial growth curve, while treatment with r*Pv*Grx5 reduced the growth rate, with the strongest inhibition observed at 200 μg/mL (Fig. 5B). Under this maximum concentration, the growth of *V. harveyi* was delayed but still reached a relatively high optical density (OD_{600}) by the end of the incubation period. A similar concentration-dependent inhibitory pattern was observed for *L. garvieae* (Fig. 5C). However, comparison of the growth kinetics between Fig. 5B and Fig. 5C revealed clear differences in the susceptibility of these two pathogens. While *V. harveyi* began to enter the exponential phase within 2 h of incubation even at 200 μg/mL, *L. garvieae* exhibited a markedly prolonged lag phase, with growth being strongly suppressed during the first 5 h of treatment at the same concentration. Furthermore, the final cell density reached by *L. garvieae* at 200 μg/mL remained substantially lower than that of *V. harveyi*. These results indicate that the growth inhibitory effect of r*Pv*Grx5 was greater in *L. garvieae* than in *V. harveyi*, particularly at higher protein concentrations.

Discussion

Glutaredoxin 5 (Grx5) is a highly conserved member of the monothiol Grx family characterized by the CGFS active-site motif and its role in cellular Fe–S cluster metabolism (Lill, 2009; Rouhier et al., 2010). In contrast to classical dithiol Grxs that primarily catalyze thiol–disulfide exchange reactions, monothiol Grxs are mainly associated with the coordination and trafficking of Fe–S clusters, which serve as essential cofactors for numerous mitochondrial and metabolic enzymes (Rodrıguez-Manzaneque et al., 2002). Through these functions, Grx5 proteins contribute to mitochondrial metabolism, intracellular iron homeostasis, and cellular redox balance. Although Grx5 proteins have been extensively characterized in several model organisms, their biological roles in crustaceans remain poorly understood. In this study, we characterized a Grx5 homolog from the white shrimp *P. vannamei* (*Pv*Grx5) and investigated its structural features, evolutionary relationships, expression patterns, and bacterial growth inhibitory activity.

Sequence analysis revealed that *Pv*Grx5 contains the conserved CGFS active-site motif, a hallmark of monothiol Grxs involved in Fe–S cluster coordination (Banci et al., 2014; Bellı et al., 2002). MSA further demonstrated strong conservation of this motif and several adjacent residues among arthropod Grx5 homologs, indicating structural conservation within this protein family (Bellı et al., 2002; Johansson et al., 2011; Rodrıguez-Manzaneque et al., 2002). Structural modeling suggested that *Pv*Grx5 adopts the characteristic Trx-like fold composed of a central β-sheet surrounded by α-helices. This structural framework is widely conserved among Grxs and

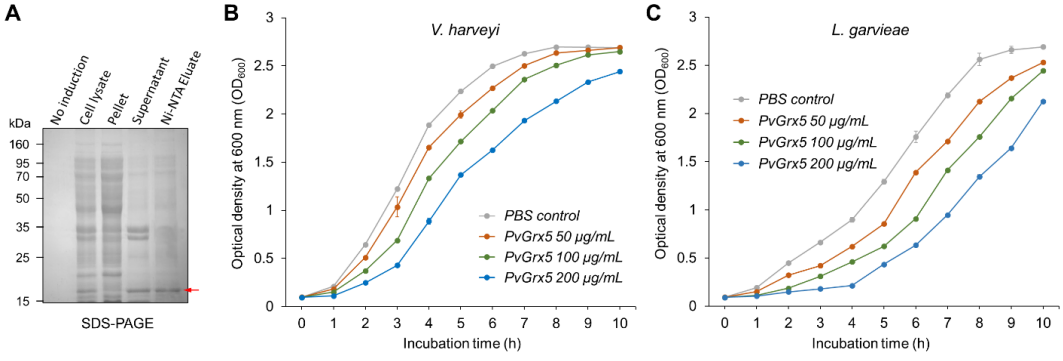

Fig. 5. Recombinant expression, purification, and bacterial growth inhibitory activity of r*Pv*Grx5. (A) SDS-PAGE (12%) analysis of r*Pv*Grx5. Growth inhibitory activity of r*Pv*Grx5 against (B) *Vibrio harveyi* and (C) *Lactococcus garvieae*. SDS-PAGE, sodium dodecyl sulfate-polyacrylamide gel electrophoresis; Ni-NTA, nickel-nitrilotriacetic acid; PBS, phosphate buffered saline; *Pv*Grx5, *Penaeus vannamei* glutaredoxin 5; r*Pv*Grx5, recombinant *Penaeus vannamei* glutaredoxin 5.

provides the catalytic environment required for GSH-dependent redox interactions (Herrero & de la Torre-Ruiz, 2007; Johansson et al., 2011). Consistent with these structural features, phylogenetic analysis grouped *Pv*Grx5 with other crustacean and arthropod Grx5 proteins, supporting its classification as a canonical member of the arthropod Grx5 lineage. The conservation of sequence motifs and structural organization suggests that *Pv*Grx5 likely retains biochemical properties associated with mitochondrial Fe–S cluster metabolism (Banci et al., 2014; Johansson et al., 2011; Lill, 2009).

The conserved architecture of *Pv*Grx5 provides insight into its potential physiological function. Monothiol Grxs containing the CGFS motif are recognized as key mediators of Fe–S cluster trafficking within the mitochondrial Fe–S cluster (ISC) assembly pathway (Lill, 2009; Rouhier et al., 2010). In this pathway, Grxs coordinate [2Fe–2S] clusters together with GSH molecules and function as intermediate carriers that transfer Fe-S clusters to recipient apoproteins involved in mitochondrial respiration and diverse metabolic processes (Banci et al., 2014; Rouhier et al., 2010). Because Fe–S proteins are essential components of many mitochondrial enzymes, disruption of this system can lead to metabolic dysfunction and disturbances in intracellular iron homeostasis. Importantly, Fe–S cluster metabolism is tightly linked to cellular redox regulation, as the assembly and maintenance of Fe–S clusters require a controlled intracellular redox environment (Rouhier et al., 2010). The structural conservation observed in *Pv*Grx5 therefore suggests that this protein may participate in coordinating mitochondrial metabolism with cellular redox homeostasis in *P. vannamei*. Although the biochemical activity of *Pv*Grx5 in Fe–S cluster transfer was not directly examined in this study, the presence of the conserved CGFS motif and Trx-like fold strongly supports its functional association with Fe–S metabolism and related redox regulatory processes.

The tissue distribution pattern of *Pv*Grx5 further supports a potential role in cellular redox regulation. *Pv*Grx5 transcripts were detected in all examined tissues, with relatively high expression observed in the gills and hemocytes. In crustaceans, gills function as major sites of respiration and environmental interaction, where continuous oxygen exchange and active ion transport can promote the generation of ROS (Goncalves et al., 2014; Henry et al., 2012). Consequently, efficient redox-regulatory systems are required to maintain cellular homeostasis in these metabolically active tissues. Hemocytes represent the primary immune effector cells in crustaceans and play central roles in pathogen recognition, phagocytosis, and antimicrobial defense (Liu et al., 2020; Söderhäll & Cerenius, 1992). During immune activation, hemocytes generate ROS as part of the oxidative burst response used to eliminate invading microorganisms. While this oxidative response is essential for host defense, excessive ROS accumulation can damage host cellular components and disrupt intracellular metabolism. Therefore, antioxidant and redox-regulatory proteins are required to maintain redox balance during immune responses. The relatively high expression of *Pv*Grx5 in hemocytes may therefore reflect its involvement in coordinating metabolic activity and redox homeostasis in immune-related tissues.

The potential involvement of *Pv*Grx5 in immune-associated redox regulation is further supported by its transcriptional response to PAMPs. *Pv*Grx5 expression was significantly induced following stimulation with LPS, PGN, and poly(I:C), suggesting that this gene is responsive to immune-related stress signals triggered by bacterial and viral mimics. In crustaceans, recognition of PAMPs typically activates innate immune responses accompanied by the rapid production of ROS, which function as an important antimicrobial defense mechanism (Holmblad & Söderhäll, 1999; Vazquez et al., 2009). Because excessive ROS accumulation can disrupt cellular metabolism and damage host tissues, redox-regulatory proteins are required to maintain intracellular redox balance during immune activation (Dickinson & Chang, 2011; Sies & Jones, 2020).

Consistent with this possibility, r*Pv*Grx5 exhibited growth inhibitory effects against the bacterial pathogens *V. harveyi* and *L. garvieae* under the experimental conditions used in this study. Notably, the more pronounced inhibitory effect observed for *L. garvieae* compared with *V. harveyi* suggests that the antimicrobial potential of r*Pv*Grx5 may be influenced by bacterial cell envelope architecture. Unlike Gram-negative bacteria *V. harveyi*, which possesses an outer membrane acting as a selective permeability barrier, the Gram-positive *L. garvieae* lack this additional lipid bilayer. This structural difference may allow r*Pv*Grx5 greater access to membrane-associated processes or iron acquisition systems that are vital for microbial fitness. In addition, monothiol Grxs are essential for the maintenance of Fe–S cluster-containing enzymes, therefore, r*Pv*Grx5 might disrupt bacterial redox-sensitive metabolic pathways by perturbing the intracellular iron homeostasis or the protein thiol pool (Banci et al., 2014; Yeung et al., 2011). Because Fe–S cluster biogenesis is tightly coupled with cellular redox balance,

https://doi.org/10.47853/FAS.2026.e29

perturbation of this pathway can impair bacterial metabolic fitness (Ayala-Castro et al., 2008; Fontecave et al., 2005). The antibacterial phenotype observed in this study—characterized by a prolonged lag phase in *L. garvieae*—may therefore reflect indirect effects on bacterial redox balance and metabolic activity rather than a direct classical antimicrobial mechanism. Nevertheless, the precise molecular mechanism underlying the antibacterial activity of *Pv*Grx5 and its *in vivo* immune functions remain to be further investigated.

Conclusion

This study presents the first molecular characterization of a Grx5 homolog in the white shrimp *P. vannamei*. The conserved CGFS motif, predicted Trx-like structural framework, and phylogenetic relationships support the classification of *Pv*Grx5 as a canonical monothiol Grx associated with Fe–S cluster metabolism. The tissue distribution and immune-inducible expression patterns further suggest that *Pv*Grx5 may participate in physiological processes linking mitochondrial metabolism, cellular redox regulation, and innate immune responses in shrimp. Moreover, the growth inhibitory effects of r*Pv*Grx5on bacterial pathogens indicate that this protein may influence host–microbe interactions through redox-associated metabolic mechanisms. Although the precise molecular mechanisms remain to be clarified, these findings expand current knowledge of Grx-mediated redox systems in crustaceans and provide a foundation for future studies investigating the roles of *Pv*Grx5 in oxidative stress regulation and immune defense in *P. vannamei*.

Competing interests

No potential conflict of interest relevant to this article was reported.

Funding sources

This work was supported by a Research Grant of Pukyong National University (2023).

Acknowledgements

Not applicable.

Availability of data and materials

The *Pv*Grx5 sequence has been deposited in GenBank under accession number PP716118.

Ethics approval and consent to participate

Not applicable.

ORCID

W. S. P. Madhuranga https://orcid.org/0000-0002-6041-4067
Chan-Hee Kim https://orcid.org/0000-0002-5315-4981

References

Almagro Armenteros JJ, Salvatore M, Emanuelsson O, Winther O, von Heijne G, Elofsson A, et al. Detecting novel sequence signals in targeting peptides using deep learning. Life Sci Alliance. 2019;2:e201900429.

Ayala-Castro C, Saini A, Wayne Outten F. Fe–S cluster assembly pathways in bacteria. Microbiol Mol Biol Rev. 2008;72:110-25.

Banci L, Brancaccio D, Ciofi-Baffoni S, Del Conte R, Gadepalli R, Mikolajczyk M, et al. [2Fe–2S] cluster transfer in iron–sulfur protein biogenesis. Proc Nat Acad Sci USA. 2014;111:6203-8.

Begas P, Liedgens L, Moseler A, Meyer AJ, Deponte M. Glutaredoxin catalysis requires two distinct glutathione interaction sites. Nat Commun. 2017;8:14835.

Bellı G, Polaina J, Tamarit J, de la Torre MA, Rodrıguez-Manzaneque MT, Ros J, et al. Structure-function analysis of yeast Grx5 monothiol glutaredoxin defines essential amino acids for the function of the protein. J Biol Chem. 2002;277:37590-6.

Cheng CH, Ma HL, Liu GX, Fan SG, Deng YQ, Feng J, et al. Identification and functional characterization of glutaredoxin 5 from the mud crab (*Scylla paramamosain*) in response to cadmium and bacterial challenge. Fish Shellfish Immunol. 2022;130:472-8.

Davies KJA. Oxidative stress, antioxidant defenses, and damage removal, repair, and replacement systems. IUBMB Life. 2000;50:279-89.

Dickinson BC, Chang CJ. Chemistry and biology of reactive oxygen species in signaling or stress responses. Nat Chem Biol. 2011;7:504-11.

Di Giulio RT, Washburn PC, Wenning RJ, Winston GW, Jewell CS. Biochemical responses in aquatic animals: a review of determinants of oxidative stress. Environ Toxicol Chem. 1989;8:1103-23.

Duan Y, Dong H, Wang Y, Li H, Liu Q, Zhang Y, et al. Intestine oxidative stress and immune response to sulfide stress in Pacific white shrimp *Litopenaeus vannamei*. Fish Shellfish Immunol. 2017;63:201-7.

Duan Y, Xiao M, Wang Y, Huang J, Yang Y, Li H. The high temperature stress responses in the hepatopancreas of *Litopenaeus vannamei*: from immune dysfunction to metabolic remodeling cascade. Front Immunol. 2025;16:1631655.

Fan J, Li B, Hong Q, Yan Z, Yang X, Lu K, et al. A glutathione peroxidase gene from *Litopenaeus vannamei* is involved in oxidative stress responses and pathogen infection resistance. Int J Mol Sci. 2022a;23:567.

Fan R, Jiang S, Li Y, Yang Q, Jiang S, Huang J, et al. Molecular characterization and expression analysis of glutaredoxin 5 in black tiger shrimp (*Penaeus monodon*) and correlation analysis between the SNPs of *Pm*Grx5 and ammonia-N stress tolerance trait. Front Mar Sci. 2022b;9:909827.

Fontecave M, Ollagnier-De-Choudens S, Py B, Barras F. Mechanisms of iron–sulfur cluster assembly: the SUF machinery. J Biol Inorg Chem. 2005;10:713-21.

Goncalves P, Guertler C, Bachère E, de Souza CRB, Rosa RD, Perazzolo LM. Molecular signatures at imminent death: hemocyte gene expression profiling of shrimp succumbing to viral and fungal infections. Dev Comp Immunol. 2014;42:294-301.

Herrero E, de la Torre-Ruiz MA. Monothiol glutaredoxins: a common domain for multiple functions. Cell Mol Life Sci. 2007;64:1518.

Henry RP, Lucu Č, Onken H, Weihrauch D. Multiple functions of the crustacean gill: osmotic/ionic regulation, acid-base balance, ammonia excretion, and bioaccumulation of toxic metals. Front Physiol. 2012;3:431.

Holmblad T, Söderhäll K. Cell adhesion molecules and antioxidative enzymes in a crustacean, possible role in immunity. Aquaculture. 1999;172:111-23.

Johansson C, Roos AK, Montano SJ, Sengupta R, Filippakopoulos P, Guo K, et al. The crystal structure of human GLRX5: iron–sulfur cluster co-ordination, tetrameric assembly and monomer activity. Biochem J. 2011;433:303-11.

Lill R. Function and biogenesis of iron–sulphur proteins. Nature. 2009;460:831-8.

Lillig CH, Berndt C, Holmgren A. Glutaredoxin systems. Biochim Biophys Acta Gen Subj. 2008;1780:1304-17.

Liao IC, Chien YH. The Pacific white shrimp, *Litopenaeus vannamei*, in Asia: the world's most widely cultured alien crustacean. In: Galil BS, Clark PF, Carlton JT, editors. In the wrong place alien marine crustaceans: distribution, biology and impacts. Dordrecht: Springer; 2011. p. 489-519.

Liu S, Zheng SC, Li YL, Li J, Liu HP. Hemocyte-mediated phagocytosis in crustaceans. Front Immunol. 2020;11:268.

Marchler-Bauer A, Derbyshire MK, Gonzales NR, Lu S, Chitsaz F, Geer LY, et al. CDD: NCBI's conserved domain database. Nucleic Acids Res. 2015;43:D222-6.

Mai HN, Caro LFA, Cruz-Flores R, White BN, Dhar AK. Differentially expressed genes in hepatopancreas of acute hepatopancreatic necrosis disease tolerant and susceptible shrimp (*Penaeus vannamei*). Front Immunol. 2021;12:634152.

Parrilla-Taylor DP, Zenteno-Savín T. Antioxidant enzyme activities in Pacific white shrimp (*Litopenaeus vannamei*) in response to environmental hypoxia and reoxygenation. Aquaculture. 2011;318:379-83.

Rouhier N, Couturier J, Johnson MK, Jacquot JP. Glutaredoxins: roles in iron homeostasis. Trends Biochem Sci. 2010;35:43-52.

Rodrıguez-Manzaneque MT, Tamarit J, Bellı G, Ros J, Herrero E. Grx5 is a mitochondrial glutaredoxin required for the activity of iron/sulfur enzymes. Mol Biol Cell. 2002;13:1109-21.

Schmittgen TD, Livak KJ. Analyzing real-time PCR data by the comparative CT method. Nat Protoc. 2008;3:1101-8.

Sun J, Hang Y, Han Y, Zhang X, Gan L, Cai C, et al. Deletion of glutaredoxin promotes oxidative tolerance and intracellular infection in *Listeria monocytogenes*. Virulence. 2019;10:910-24.

Sies H, Jones DP. Reactive oxygen species (ROS) as pleiotropic physiological signalling agents. Nat Rev Mol Cell Biol. 2020;21:363-83.

Sies H, Belousov VV, Chandel NS, Davies MJ, Jones DP, Mann GE, et al. Defining roles of specific reactive oxygen species (ROS) in cell biology and physiology. Nat Rev Mol Cell Biol. 2022;23:499-515.

Söderhäll K, Cerenius L. Crustacean immunity. Ann Rev Fish Dis. 1992;2:3-23.

Tamura K, Stecher G, Kumar S. MEGA11: molecular evolutionary genetics analysis version 11. Mol Biol Evol. 2021;38:3022-7.

Trnka D, Engelke AD, Gellert M, Moseler A, Hossain MF, Lindenberg TT, et al. Molecular basis for the distinct functions of redox-active and FeS-transfering glutaredoxins. Nat Commun. 2020;11:3445.

Vazquez L, Alpuche J, Maldonado G, Agundis C, Pereyra-Morales A, Zenteno E. Immunity mechanisms in crustaceans. Innate Immun. 2009;15:179-88.

Xu Z, Regenstein JM, Xie D, Lu W, Ren X, Yuan J, et al. The oxidative stress and antioxidant responses of *Litopenaeus vannamei* to low temperature and air exposure. Fish Shellfish Immunol. 2018;72:564-71.

Yeung N, Gold B, Liu NL, Prathapam R, Sterling HJ, Willams

https://doi.org/10.47853/FAS.2026.e29

ER, et al. The *E. coli* monothiol glutaredoxin GrxD forms homodimeric and heterodimeric FeS cluster containing complexes. Biochemistry. 2011;50:8957-69.

Yu CS, Cheng CW, Su WC, Chang KC, Huang SW, Hwang JK, et al. CELLO2GO: a web server for protein subCELlular LOcalization prediction with functional gene ontology annotation. PLOS ONE. 2014;9:e99368.